Exact Stoichiometry of CexZr6–x Cornerstones in Mixed-Metal UiO-66 Metal–Organic Frameworks Revealed by Extended X-ray Absorption Fine Structure Spectroscopy

Exact stoichiometry of Ce_xZr_{6-x} cornerstones in mixed-metal UiO-66 MOFs revealed by EXAFS spectroscopy

Kirill A. Lomachenko,*[,1] Jannick Jacobsen,[2] Aram L. Bugaev,[3] Cesare Atzori,[4] Francesca Bonino,[4] Silvia Bordiga,[4] Norbert Stock,[2] and Carlo Lamberti*[,3,5]

1) European Synchrotron Radiation Facility, 71 Avenue des Martyrs, CS 40220, 38043 Grenoble Cedex 9, France
2) Institut für Anorganische Chemie, Christian-Albrechts-Universität, Max-Eyth-Straße 2, D 24118 Kiel, Germany
3) "The Smart Materials Research Center", Southern Federal University, Sladkova 178/24, 344090 Rostov-on-Don, Russia
4) Department of Chemistry, NIS interdepartmental Center and INSTM Reference Center, University of Turin, Via Quarello 15, 10135 Turin, Italy
5) Department of Physics, INSTM Reference Center and CrisDi Interdepartmental Centre for Crystallography, University of Turin, Via P. Giuria 1, 10125 Turin Italy

Abstract

Recently synthesized bimetallic Ce/Zr-UiO-66 MOFs proved to be a promising material for various catalytic redox applications, representing, together with other bimetallic MOFs, a new generation of porous materials. However, no direct proof for the presence of both metals in a single cornerstone of UiO-type MOFs was reported so far. Employing element-selective XAS techniques herein we demonstrate for the first time that our synthesis route allows obtaining Ce/Zr-UiO-66 MOFs with desired Ce content and bimetallic $CeZr_5$ cornerstones. Performing multiple-edge EXAFS analysis we determine the exact stoichiometry of the cornerstones, which explains the dependence of thermal and chemical stability of the materials on Ce content.

Introduction

Metal-Organic Frameworks (MOFs) are porous compounds with high specific surface area, tuneable pore sizes and different chemical functionalities. They are formed by the connection of inorganic and organic building units through coordinative bonding.[1-2] Zirconium-based MOFs have attracted substantial interest since the first Zr-MOF UiO-66, $[Zr_6(\mu_3\text{-}O)_4(\mu_3\text{-}OH)_4(BDC)_6]$ with BDC^{2-} = 1,4-benzenedicarboxylate, has been reported (Figure 1a).[3] The structure of most Zr-MOFs contain hexanuclear $[Zr_6(\mu_3\text{-}O)_4(\mu_3\text{-}OH)_4]^{12+}$ clusters

which are connected by di-, tri- or tetra-carboxylate linker molecules to form two- or three-dimensional networks.[3-7]

Being exceptionally stable,[3-4, 6] Zr clusters (Figure 1b) are not very active chemically due to the limited redox capabilities of Zr. In contrast, cerium is known for a wide range of catalytic applications.[8] To combine the stability and porosity of UiO-66 structure with the redox properties of Ce metal, we have recently accomplished the first successful synthesis of pure Ce-UiO-66 employing linker molecules of various sizes and functional groups.[9] Such MOFs have already been studied by us and other groups in various catalytical applications.[9-12] In a recent study, Smolders et al. demonstrated that one cerium atom per hexanuclear Ce_6 cluster in UiO-67 MOF is indeed redox-active and switches the oxidation state between Ce(III)/Ce(IV).[13]

To further improve the performance of Ce-UiO MOFs in terms of stability, which is still inferior to those of pure Zr-UiO-66,[3-4, 6] we started to investigate the synthesis and properties of mixed-metal Ce/Zr-MOFs. As a result, an increased thermal and chemical stability compared to pure Ce-UiO-66 was observed for mixed-metal compounds containing low amounts of Ce(IV) ions (< 20% of total metal content), reaching up to 350 °C for the mixed-metal $Ce_{0.5}Zr_{5.5}$UiO-66 MOF.[14] Other groups have also reported the synthesis of Ce-containing Zr-UiO-66 MOF and successfully employed it in catalytic studies.[15-16]

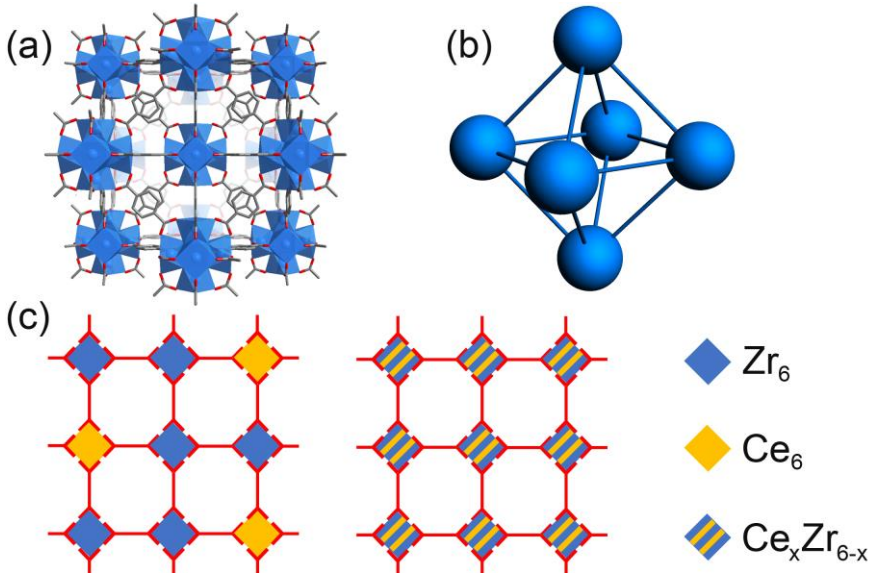

Figure 1 (a) Fragment of crystal structure of UiO-66 MOF, showing BDC linkers and $Zr_6(\mu_3\text{-}O)_4(\mu_3\text{-}OH)_4$ cornerstones; (b) Closeup on UiO-66 cornerstone (M atoms only); (c-d) Schematic representation of mixed-metal Ce_xZr_{6-x}-UiO-66 structure with pure (c) and bimetallic cornerstones (d).

Although the metal substitution in different MOFs is widely discussed in the literature,[17-27] to the best of our knowledge, no direct proof for the existence of mixed-metal cornerstones in UiO-family MOFs have been presented so far. While extra-phases present in the framework pores may be detected by powder X-ray diffraction (PXRD)[16] or N_2 physisorption,[28] in their absence the cornerstones in the mixed-metal compounds were only assumed to be either pure (e.g. Zr/Ti- and Zr/Hf-UiO-66 MOFs)[29] or truly bimetallic

(e.g. CeZr-UiO-66 MOF)[15], as shown in panels c and d of Figure 1, respectively. However, no discussion regarding the discrimination of these chemically different cases was provided.

The key to the quantitative determination of the cornerstone composition is the use of element-selective techniques, since the fine non-periodic variations of local atomic structure can hardly be detected by non-selective scattering-based methods. In this study, we provide the first direct proof of the existence of mixed-metal Ce/Zr cornerstones in Ce_xZr_{6-x}-UiO-66 MOF, possible due to the combined analysis of Zr and Ce K-edge EXAFS data for the series of samples with different Ce content, coupled with complementary techniques.

The synthesis of the pure Ce-UiO-66 and mixed-metal Ce/Zr-UiO-66 compounds was performed following the procedure reported by Lammert et al.[9, 14], whereas pure Zr-UiO-66 was prepared as described in the work of Cavka et al. [3] (SI, Section 1). Ce content in all compounds was determined by energy-dispersive X-ray spectroscopy (SI, Section 2 and Table S2). The mixed-metal samples will be referred to as CeXX in the discussion of the EXAFS results, XX being the fraction of Ce in the total metal content of the MOF (in mol. %) determined by EDX.

Synchrotron PXRD measurements for desolvated pure Zr-, pure Ce- and bimetallic $Zr_{3.54}Ce_{2.46}$-UiO-66 MOFs were performed at ID22 beamline of the European Synchrotron Radiation Facility (ESRF) to determine with high precision their structural parameters, further used as the initial guess for the EXAFS refinement.

As a general tendency, the peak width decreases upon incorporation of Ce into the structure, thus the narrowest peaks were observed in the PXRD patterns of Ce-UiO-66 while Zr-UiO-66 exhibited the broadest ones, indicating the progressive increase of crystallite size with the rise of Ce content. The patterns indicate no symmetry-forbidden additional peaks due to nano-regions containing correlated lattice defects with reo topology[30] and are in perfect agreement with the *Fm*-3*m* space group (Figures S1-3 and Table S3). Hence, both Ce and Zr atoms, as well as the cluster and/or linker vacancies for all the investigated samples are randomly distributed throughout the crystal. The occurrence of large domains with lower crystalline symmetry, as well as the formation of crystalline extra-phases, is thus ruled out. Concomitantly, TGA and BET measurements reported by Lammert et al.[14] for analogous CeZr-UiO-66 MOFs evidenced that substitution of Zr with Ce is not accompanied by a significant rise of missing linker defects, resulting in a maximum of 1 missing linker per cornerstone. Thus, it is not the defects, but the local composition of the clusters that has the major influence on the EXAFS data discussed below.

Ce and Zr K-edge EXAFS as well as Ce L_3 XANES spectra were collected at BM31[31] (Ce22, Ce45 and Ce84 and pure Ce and Zr UiO-66 MOFs) and BM23[32] (Ce10 MOF) beamlines of ESRF, measuring as-prepared compounds at room temperature. Ce L_3-edge XANES data for all Ce-containing samples show the pure Ce(IV) phase (indicatively more than 95% of Ce content), confirming the success of the synthesis (Figure S4a). Differences between the XANES spectra of all MOFs at the three edges were minor, indicating that

the electronic structure of neither Ce nor Zr species was significantly altered at different Ce:Zr ratios and excluding the possibility to draw structural conclusions from the in-depth XANES analysis (Figure S4).

Fourier-transformed Zr and Ce K-edge EXAFS data for all MOFs are shown in the Figure S6. Qualitatively the spectra are in agreement with those reported previously for Zr-UiO-66 MOFs[4, 33] and for Ce complexes with the geometry similar to the UiO-type cornerstones.[34] The shape of the peaks in 1.2-2.5 Å range, originating mainly from M–O scattering (M being Zr or Ce), does not change significantly upon the increase of Ce content, which evidences rather small variations in O-coordination of Zr and Ce atoms. However, very pronounced changes are observed in the position and intensity of the second peak (2.8-3.8 Å), which appears due to the M–M scattering from the members of M_6 cornerstones (Figure 1b). It clearly indicates that the average values of M–M interatomic distances, as well as the corresponding disorder, depend on Ce:Zr ratio, which confirms the formation of mixed-metal Ce_xZr_{6-x} cornerstones.

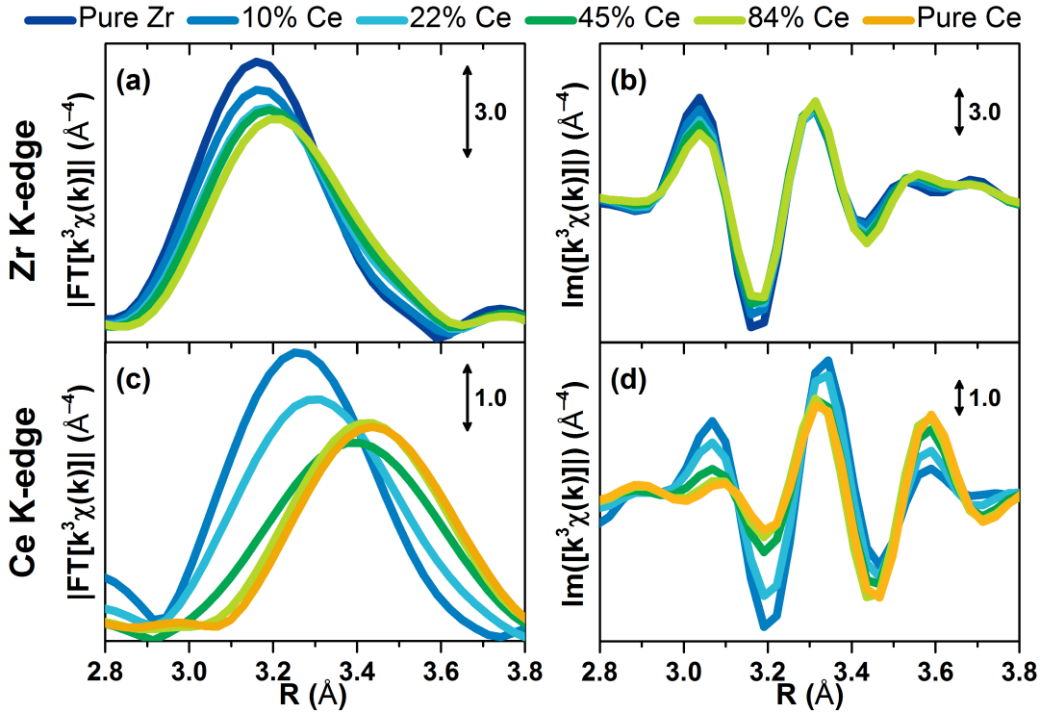

Figure 2 Closeup on the second shell peak in the modulus (a,c) and imaginary part (b,d) of phase-uncorrected Fourier transforms of k^3-weighted EXAFS data collected at Zr (a,b) and Ce K-edges (c,d) for the pure and mixed-metal UiO-66 MOFs.

Figure 2a,c presents a closeup on the second EXAFS peak of all the studied MOFs, which simplifies a comparative rationalization of the data and allows to qualitatively explain the observed trends. Changes that take place upon introduction of Ce may be explained by assuming the preferential formation of $CeZr_5$ clusters, accompanied by pure Zr_6 or Ce_6 cornerstones in the proportion dictated by the total stoichiometry of the sample. This implies a coexistence of $CeZr_5$ and Zr_6 clusters for Ce contents lower than 17% (i.e. 1/6) and a mixture of $CeZr_5$ and Ce_6 for higher Ce loadings.

For the pure Zr MOF, the Zr–Zr distances in the cornerstones are highly homogeneous, leading to the maximum intensity of the Zr-Zr peak in the absence of static disorder. Upon the introduction of Ce, the formation of $CeZr_5$ clusters would cause progressive loss of intensity at Zr K-edge compared to the pure

Zr MOF due to the splitting of the Zr–Zr coordination shell into Zr-Ce and Zr-Zr subshells with significantly different Zr–M distances, in agreement to the data for Ce10 and Ce22 samples (Figure 2a). The minimum should be reached at Ce content around 17%, when all of the cornerstones are represented by the $CeZr_5$ clusters. At the same time, at the Ce K-edge the intensity of the Ce–M peak would be at its maximum for low-Ce samples, since static and dynamic disorder of the Ce–Zr distances in the $CeZr_5$ clusters is expected to be quite low and comparable to the one of Zr–Zr in pure Zr clusters, while the Ce–Zr distance is likely to be shorter than the Ce–Ce one. For Ce loadings higher than 17%, the data evidence against the formation of mixed clusters with more than 1 Ce atom, but rather suggest that mainly pure Ce_6 cornerstones are formed from the excess of Ce, in addition to the $CeZr_5$ clusters. Indeed, that would explain the lack of major changes at the Zr K-edge between Ce22, Ce45 and Ce84 samples, since in such a case all the Zr atoms in the material would be present as a part of $CeZr_5$ cornerstones and it is only the abundance of such cornerstones that would change with the increase of Ce content, but not their composition. Concomitantly, pure Ce_6 clusters are expected to have longer and less homogenous Ce–Ce distances compared to Ce–Zr and Zr–Zr ones in Zr_6 and $CeZr_5$ clusters, resulting in a shift of the second EXAFS peak at Ce K-edge to higher R and a decrease of its intensity.

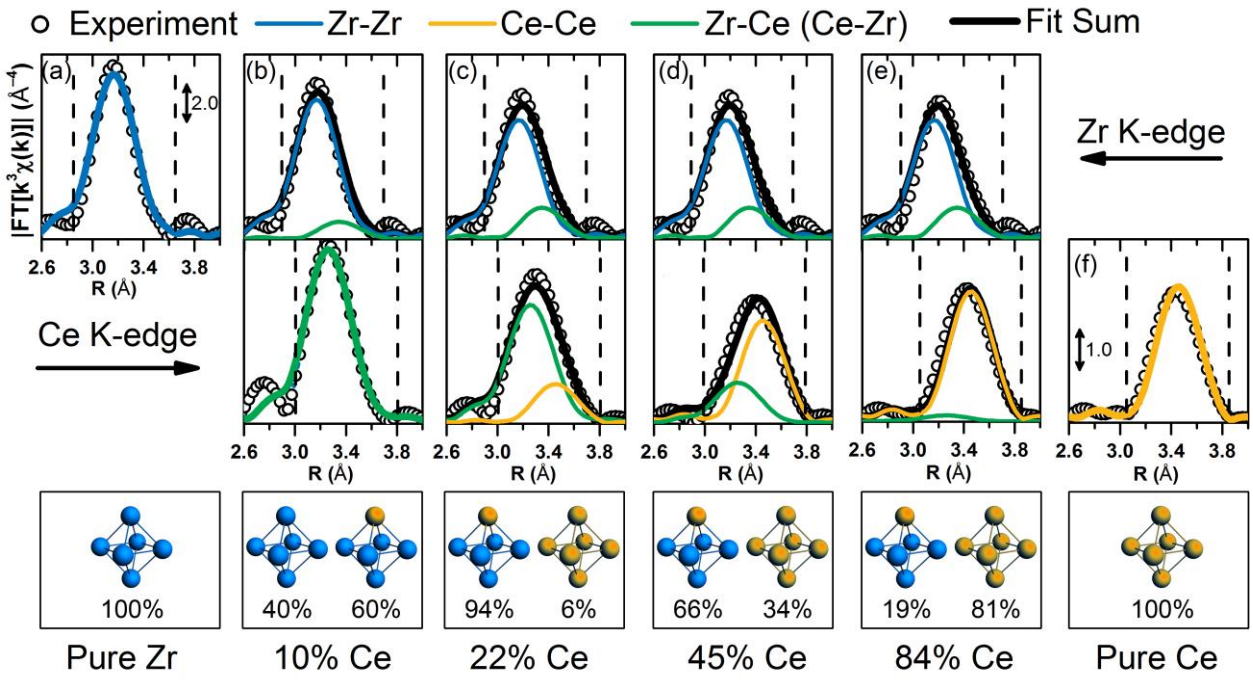

Figure 3 Results of the EXAFS fitting. Experimental data are shown as white circles, fitted curves are presented as full lines. Color code: Zr–Zr contribution – blue, Ce–Ce contribution – yellow, Zr–Ce and Ce-Zr contribution – green. For mixed-metal MOFs the sum of the two contributions is shown in black. Bottom panels summarize the cornerstone composition employed for fitting the spectra of each sample.

Imaginary parts of the Ce K-edge EXAFS Fourier transforms (Figure 2d) indicate that it is the relative abundance of contributing Ce–Zr and Ce–Ce paths that changes at different Ce content rather than the lengths of these paths. Indeed, no shift of the oscillations is observed upon the increase of Ce content,

but rather the redistribution of the intensity from R = 3.1 Å region, where contribution of Ce–Zr scattering should be dominant, to R = 3.6 Å, where Ce–Ce signal is the strongest (given distances are not phase-corrected).

Table 1 Best-fit parameters obtained by combined EXAFS fitting of eight datasets at both Zr and Ce K-edges. M–M interatomic distances obtained from PXRD refinement are shown in parentheses.

Parameter	Value
R-factor	0.012
N_{ind}	63.1
N_{par}	11
S_0^2	1.0 ± 0.1
ΔE_{Ce}, eV	0.9 ± 1.1
ΔE_{Zr}, eV	0.6 ± 0.7
$R_{Ce\text{-}Zr}$, Å	3.653 ± 0.004 (3.67)
$\sigma^2_{Ce\text{-}Zr}$, Å^2	0.0050 ± 0.0002
$R_{Ce\text{-}Ce}$, Å^2	3.784 ± 0.004 (3.78)
$\sigma^2_{Ce\text{-}Ce}$, Å^2	0.0060 ± 0.0002
$R_{Zr\text{-}Zr}$, Å	3.529 ± 0.003
$\sigma^2_{Zr\text{-}Zr}$, Å^2	0.0050 ± 0.0002
R_{Zr6}	3.525 ± 0.003 (3.51)
σ^2_{Zr6}, Å^2	0.0046 ± 0.0002
|Highest correlations|	$\Delta R_{Zr\text{-}Zr}/\Delta E_{Zr}$ = 0.89
	$\Delta R_{Ce\text{-}Ce}/\Delta E_{Ce}$ = 0.85
	$\Delta R_{Zr6}/\Delta E_{Zr}$ = 0.85
	$\sigma^2_{Zr\text{-}Zr}/S_0^2$ = 0.84
	σ^2_{Zr6}/S_0^2 = 0.83
	$\Delta R_{Ce\text{-}Zr}/\Delta E_{Ce}$ = 0.83
	others < 0.8

Hypothesis about the preferential formation of $CeZr_5$ cornerstones, put forward after the qualitative analysis of the EXAFS data was confirmed by quantitative EXAFS fitting at Zr and Ce K-edges. All ten EXAFS datasets (five at each edge) were fitted together, leading to the calculation of a global R-factor. Degeneracies of M–M paths for bimetallic MOFs were calculated from the elemental composition data provided by EDX analysis assuming preferential formation of the $CeZr_5$ cornerstones (SI, Section 4.4). Results of the combined EXAFS fitting of ten independent datasets are shown in Figure 3, while the values of the obtained fitting parameters are reported in Table 1.

The fit shows excellent overall agreement with the experiment, especially given the large amount of data and a set of physical constraints applied during parametrization (see SI Section 4.4 for details). Obtained DW factors demonstrate that the extent of structural disorder depends on the composition of the cluster. The lowest DW factor σ^2_{Zr6} = 0.0046 Å^2 was obtained for the Zr-Zr path in pure Zr_6 cornerstones, which were expected to be the most rigid and ordered ones. Inclusion of one Ce atom in the cornerstone increases very slightly the inhomogeneity of the Zr-Zr and Zr-Ce distances, justifying the small rise of the corresponding DW factors to $\sigma^2_{Zr\text{-}Zr} = \sigma^2_{Ce\text{-}Zr}$ = 0.0050 Å^2. Apart from the low values of the DW factors, rather low degree of disorder in metal-metal distances of both the Zr_6 and the $CeZr_5$ clusters is confirmed also

by the presence of the peak at R = 4.5-5 Å in the Zr K-edge EXAFS FT (see Figure S6a). This peak originates due to the scattering from the M atom, situated in the opposite vertex of the octahedron with respect to the absorbing atom (Figure 1b)[4-5, 35]. At the Ce K-edge EXAFS FT this peak is distinguishable from the noise only for Ce10 and Ce22 samples, where the majority of Ce atoms are part of $CeZr_5$ cornerstones, while in the MOFs with higher Ce content it is below the noise level, which implies higher disorder in Ce_6 clusters compared to Zr_6 and $CeZr_5$ ones. Concomitantly, the EXAFS fit results in DW factor $\sigma^2_{Ce\text{-}Ce}$ = 0.0060 Å^2 for the Ce–Ce path, which is roughly 20 % higher compared to those for Zr–Zr and Zr–Ce pairs.

The preferential formation of $CeZr_5$ cornerstones explains the trends in the stability of bimetallic UiO-66 MOFs with different Ce content reported recently by Lammert et al.[14] Indeed, while at low Ce loadings stability was decreasing linearly with the increase of Ce content, at around 20% it stabilized at the value observed for pure Ce-UiO-66 MOF. According to the current EXAFS analysis, this coincides with the disappearance of pure Zr_6 cornerstones, which, due to lower disorder and higher stability compared to Ce_6 and $CeZr_5$ cornerstones, increase the decomposition temperature of the material.

The preferential formation of $CeZr_5$ cornerstones over the other mixed-metal clusters is partially in line with the recent theoretical calculations of Trousselet et al.,[36] that show that as a general trend, the mixing energy of the bimetallic cluster increases with the number of bimetallic edges. However, the mixing energy for all possible structure of Ce_xZr_{6-x} cornerstone was reported to be positive, suggesting that in principle the most favorable configuration for Ce/Zr-UiO-66 MOF would be the structure with only Zr_6 and Ce_6 cornerstones. Our DFT calculations also evidence that energetically the most favorable way to accommodate Ce atoms in the structure would be the formation of Ce_6 cornerstones (SI Section 5). In such case, though, the Ce and Zr K-edge EXAFS spectra at different Ce loadings would be identical, which is clearly not the case. Therefore, the formation of the MOF structure is likely to have more complex drivers, which might require the inclusion of additional factors (temperature, pressure, solvent effects) into the computational model to correctly account for them in the calculations. The high level of complexity of this challenging computational task highlights the value of the experimental methods for the determination of the composition of bimetallic MOFs.

To summarize, combined Ce and Zr K-edge EXAFS analysis demonstrates that in bimetallic Ce/Zr-UiO-66 MOFs mixed-metal $CeZr_5$ cornerstones coexist with pure Zr_6 (at Ce content lower than ca. 20%) and Ce_6 ones (at higher Ce content). The relative abundance of pure and bimetallic cornerstones is in both cases determined primarily by sample stoichiometry. Such observation serves as a first direct proof for the existence of mixed ZrCe cornerstones in the Ce/Zr-UiO-66 MOF and allows to explain the previously-reported non-trivial dependence of temperature stability of these MOFs on Ce content.

Acknowledgements

The authors are grateful to M. Brunelli, H. Emerich, W. van Beek, V. Dmitriev, O. Mathon and A. Fitch for the support during the experiments at BM31, BM23 and ID22 beamlines of the ESRF. We would like to

thank B. Bueken, S. Smolders and A. Venier for the help with the XAS measurements, and H. Reinsch and N. Heidenreich for the assistance with PXRD experiment and data analysis. ALB acknowledges the grant of the Southern Federal University VnGr-07/2017-08.

References

(1) Yaghi, O. M.; O'Keeffe, M.; Ockwig, N. W.; Chae, H. K.; Eddaoudi, M.; Kim, J., *Nature* **2003**, *423*, 705.
(2) Butova, V. V.; Soldatov, M. A.; Guda, A. A.; Lomachenko, K. A.; Lamberti, C., *Russ. Chem. Rev.* **2016**, *85*, 280-307.
(3) Cavka, J. H.; Jakobsen, S.; Olsbye, U.; Guillou, N.; Lamberti, C.; Bordiga, S.; Lillerud, K. P., *J. Am. Chem. Soc.* **2008**, *130*, 13850-13851.
(4) Valenzano, L.; Civalleri, B.; Chavan, S.; Bordiga, S.; Nilsen, M. H.; Jakobsen, S.; Lillerud, K. P.; Lamberti, C., *Chem. Mater.* **2011**, *23*, 1700-1718.
(5) Chavan, S.; Vitillo, J. G.; Gianolio, D.; Zavorotynska, O.; Civalleri, B.; Jakobsen, S.; Nilsen, M. H.; Valenzano, L.; Lamberti, C.; Lillerud, K. P.; Bordiga, S., *Phys. Chem. Chem. Phys.* **2012**, *14*, 1614-1626.
(6) Shearer, G. C.; Chavan, S.; Ethiraj, J.; Vitillo, J. G.; Svelle, S.; Olsbye, U.; Lamberti, C.; Bordiga, S.; Lillerud, K. P., *Chem. Mater.* **2014**, *26*, 4068-4071.
(7) Øien, S.; Wragg, D.; Reinsch, H.; Svelle, S.; Bordiga, S.; Lamberti, C.; Lillerud, K. P., *Cryst. Growth Des.* **2014**, *14*, 5370-5372.
(8) Montini, T.; Melchionna, M.; Monai, M.; Fornasiero, P., *Chem. Rev.* **2016**, *116*, 5987-6041.
(9) Lammert, M.; Wharmby, M. T.; Smolders, S.; Bueken, B.; Lieb, A.; Lomachenko, K. A.; Vos, D. D.; Stock, N., *Chem. Commun.* **2015**, *51*, 12578-12581.
(10) Dalapati, R.; Sakthivel, B.; Ghosalya, M. K.; Dhakshinamoorthy, A.; Biswas, S., *CrystEngComm* **2017**, *19*, 5915-5925.
(11) Dalapati, R.; Sakthivel, B.; Dhakshinamoorthy, A.; Buragohain, A.; Bhunia, A.; Janiak, C.; Biswas, S., *CrystEngComm* **2016**, *18*, 7855-7864.
(12) Buragohain, A.; Biswas, S., *CrystEngComm* **2016**, *18*, 4374-4381.
(13) Smolders, S.; Lomachenko, K. A.; Bueken, B.; Struyf, A.; Bugaev, A. L.; Atzori, C.; Stock, N.; Lamberti, C.; Roeffaers, M. B. J.; De Vos, D. E., *ChemPhysChem* **2018**, *19*, 373-378.
(14) Lammert, M.; Glißmann, C.; Stock, N., *Dalton Trans.* **2017**, *46*, 2425-2429.
(15) Nouar, F.; Breeze, M. I.; Campo, B. C.; Vimont, A.; Clet, G.; Daturi, M.; Devic, T.; Walton, R. I.; Serre, C., *Chem. Commun.* **2015**, *51*, 14458-14461.
(16) Ebrahim, A. M.; Bandosz, T. J., *ACS Appl. Mater. Interfaces* **2013**, *5*, 10565-10573.
(17) Liu, Q.; Cong, H.; Deng, H., *J. Am. Chem. Soc.* **2016**, *138*, 13822-13825.
(18) Lee, Y.; Kim, S.; Kang, J. K.; Cohen, S. M., *Chem. Commun.* **2015**, *51*, 5735-5738.
(19) He, J.; Zhang, Y.; He, J.; Zeng, X.; Hou, X.; Long, Z., *Chem. Commun.* **2018**, *54*, 8610-8613.
(20) Tu, J.; Zeng, X.; Xu, F.; Wu, X.; Tian, Y.; Hou, X.; Long, Z., *Chem. Commun.* **2017**, *53*, 3361-3364.
(21) Szeto, K. C.; Lillerud, K. P.; Tilset, M.; Bjørgen, M.; Prestipino, C.; Zecchina, A.; Lamberti, C.; Bordiga, S., *J. Phys. Chem. B* **2006**, *110*, 21509-21520.
(22) Szeto, K. C.; Prestipino, C.; Lamberti, C.; Zecchina, A.; Bordiga, S.; Bjørgen, M.; Tilset, M.; Lillerud, K. P., *Chem. Mater.* **2007**, *19*, 211-220.
(23) Brozek, C. K.; Dincă, M., *J. Am. Chem. Soc.* **2013**, *135*, 12886-12891.
(24) Brozek, C. K.; Dincă, M., *Chem. Soc. Rev.* **2014**, *43*, 5456-5467.
(25) Vuong, G.-T.; Pham, M.-H.; Do, T.-O., *Dalton Trans.* **2013**, *42*, 550-557.
(26) Stubbs, A. W.; Braglia, L.; Borfecchia, E.; Meyer, R. J.; Román- Leshkov, Y.; Lamberti, C.; Dincă, M., *ACS Catal.* **2018**, *8*, 596-601.
(27) Butova, V. V.; Polyakov, V. A.; Budnyk, A. P.; Aboraia, A. M.; Bulanova, E. A.; Guda, A. A.; Reshetnikova, E. A.; Podkovyrina, Y. S.; Lamberti, C.; Soldatov, A. V., *Polyhedron* **2018**, *154*, 457-464.
(28) Santaclara, J. G.; Olivos-Suarez, A. I.; Gonzalez-Nelson, A.; Osadchii, D.; Nasalevich, M. A.; van der Veen, M. A.; Kapteijn, F.; Sheveleva, A. M.; Veber, S. L.; Fedin, M. V.; Murray, A. T.; Hendon, C. H.; Walsh, A.; Gascon, J., *Chem. Mater.* **2017**, *29*, 8963-8967.
(29) Kim, M.; Cahill, J. F.; Fei, H.; Prather, K. A.; Cohen, S. M., *J. Am. Chem. Soc.* **2012**, *134*, 18082-18088.
(30) Cliffe, M. J.; Wan, W.; Zou, X.; Chater, P. A.; Kleppe, A. K.; Tucker, M. G.; Wilhelm, H.; Funnell, N. P.; Coudert, F.-X.; Goodwin, A. L., *Nat. Commun.* **2014**, *5*, 4176.
(31) Abdala, P. M.; Safonova, O. V.; Wiker, G.; van Beek, W.; Emerich, H.; van Bokhoven, J. A.; Sá, J.; Szlachetko, J.; Nachtegaal, M., *CHIMIA* **2012**, *66*, 699-705.
(32) Mathon, O.; Beteva, A.; Borrel, J.; Bugnazet, D.; Gatla, S.; Hino, R.; Kantor, I.; Mairs, T.; Munoz, M.; Pasternak, S.; Perrin, F.; Pascarelli, S., *J. Synchrotron Rad.* **2015**, *22*, 1548-1554.
(33) Plonka, A. M.; Wang, Q.; Gordon, W. O.; Balboa, A.; Troya, D.; Guo, W.; Sharp, C. H.; Senanayake, S. D.; Morris, J. R.; Hill, C. L.; Frenkel, A. I., *J. Am. Chem. Soc.* **2017**, *139*, 599-602.
(34) Hennig, C.; Ikeda-Ohno, A.; Kraus, W.; Weiss, S.; Pattison, P.; Emerich, H.; Abdala, P. M.; Scheinost, A. C., *Inorg. Chem.* **2013**, *52*, 11734-11743.
(35) Jakobsen, S.; Gianolio, D.; Wragg, D. S.; Nilsen, M. H.; Emerich, H.; Bordiga, S.; Lamberti, C.; Olsbye, U.; Tilset, M.; Lillerud, K. P., *Phys. Rev. B* **2012**, *86*, 125429.
(36) Trousselet, F.; Archereau, A.; Boutin, A.; Coudert, F.-X., *J. Phys. Chem. C* **2016**, *120*, 24885-24894.